

Gradient Regularization-based Neural Granger Causality

Meiliang Liu¹, Donghui Wen¹, Xiaoxiao Yang¹, Yunfang Xu¹, Zijin Li¹, Zhengye Si¹, Xinyue Yang¹, Zhiwen Zhao¹

¹School of Artificial Intelligence, Beijing Normal University, Beijing, China

Abstract

With the advancement of deep learning technologies, various neural network-based Granger causality models have been proposed. Although these models have demonstrated notable improvements, several limitations remain. Most existing approaches adopt the component-wise architecture, necessitating the construction of a separate model for each time series, which results in substantial computational costs. In addition, imposing the sparsity-inducing penalty on the first-layer weights of the neural network to extract causal relationships weakens the model’s ability to capture complex interactions. To address these limitations, we propose Gradient Regularization-based Neural Granger Causality (GRNGC), which requires only one time series prediction model and applies L_1 regularization to the gradient between model’s input and output to infer Granger causality. Moreover, GRNGC is not tied to a specific time series forecasting model and can be implemented with diverse architectures such as KAN, MLP, and LSTM, offering enhanced flexibility. Numerical simulations on DREAM, Lorenz-96, fMRI BOLD, and CausalTime show that GRNGC outperforms existing baselines and significantly reduces computational overhead. Meanwhile, experiments on real-world DNA, Yeast, HeLa, and bladder urothelial carcinoma datasets further validate the model’s effectiveness in reconstructing gene regulatory networks.

Introduction

Granger causality is a widely adopted method for causal inference in time series analysis. It examines whether the historical values of one variable can statistically enhance the prediction of another variable’s future values. Different from correlation-based methods, which only capture synchronous activities between variables, Granger causality can identify the temporal order and directional dependence between variables. This distinctive capability facilitates its applications across various complex systems, including financial markets, climate systems, and effective connectivity modelling in neuroimaging.

With the advent of deep learning, various neural network-based Granger causality models have been proposed. Tank et al. (2018) propose the component-wise Multilayer Perceptron and Long Short-Term Memory (cMLP & cLSTM), extracting the first-layer weights of MLP/LSTM and applying the sparsity-inducing penalty to infer causal relationships. Subsequent studies include economy statistical recur-

rent units (eSRU), Causal Discovery from Irregular Time Series (CUTS), and Jacobian Granger causality (JGC), etc. Although these models have made improvements, several limitations remain to be addressed: (1) Most existing models rely on the component-wise architecture, which requires training a separate model for each time series, resulting in high computational costs. (2) Causal relationships are often inferred from the first-layer weights of neural networks. However, this strategy becomes insufficient in high-dimensional time series, since the search space for causal variance becomes broader and may converge to local optima. (3) The complex architecture with numerous parameters hinders the scalability of these models.

Motivated by these challenges, we aim to propose a neural Granger causality framework that eliminates the need for the component-wise architecture by using a single model. Our second objective is to design a simple and flexible architecture that can be constructed using various time series prediction models, thereby ensuring scalability and flexibility. Lastly, we plan to introduce a novel method for inferring causal relationships that extends beyond conventional approaches, which rely solely on the first-layer weights of the neural network.

In this paper, we propose Gradient Regularization-based Neural Granger Causality (GRNGC) for time series Granger causality inference. Our contributions are as follows:

- We propose a novel Granger causality model, termed GRNGC, which employs a Kolmogorov-Arnold network (can be replaced by other time series prediction models) and incorporates L_1 regularization on the input-output gradient to extract causal relationships.
- Numerical simulations demonstrate that GRNGC outperforms existing baselines on DREAM, Lorenz-96, fMRI BOLD signals, and CausalTime datasets, while also achieving notable reductions in computational overhead.
- Experiments on *SOS DNA repair network*, *Yeast*, *HeLa*, and *Bladder Urothelial Carcinoma* datasets further validate the effectiveness of GRNGC in reconstructing real-world gene regulatory networks.

Related Work

Recently, neural network-based approaches for inferring Granger causality from nonlinear time series have gained

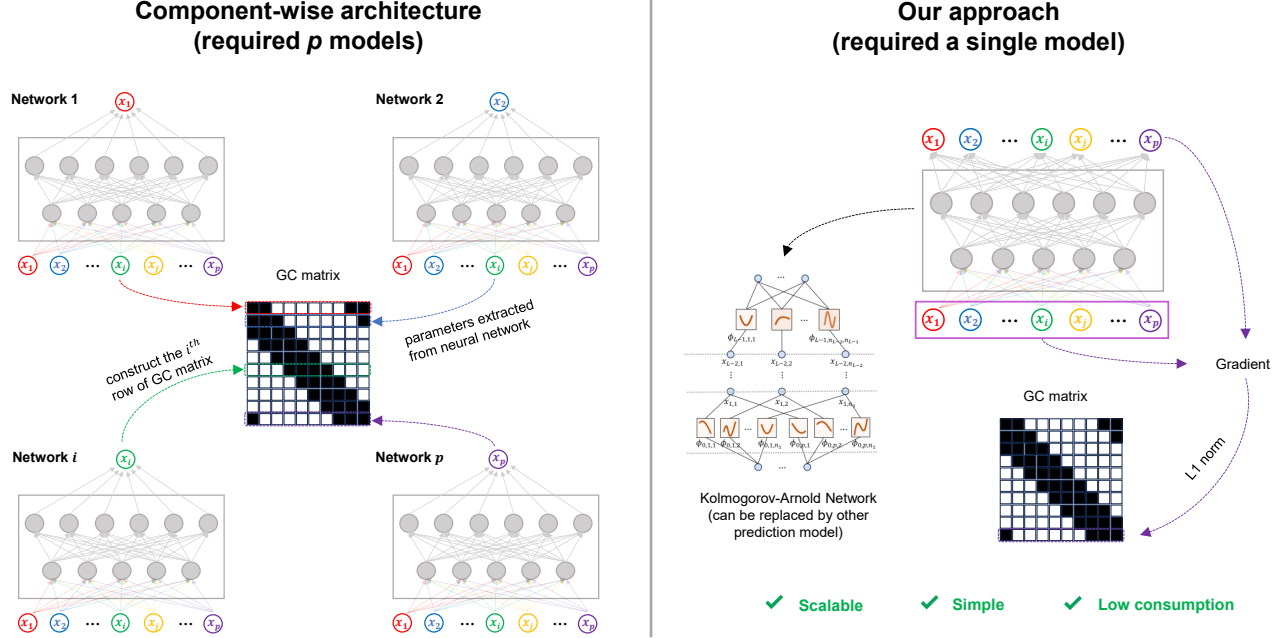


Figure 1: (Left) Previous component-wise architecture, which required p models for p -dimensional time series. (Right) The architecture of proposed GRNGC, which only required one model for p -dimensional time series.

significant attention. Tank et al. (2018) proposed cMLP and cLSTM, which utilized the first-layer weights of MLP and LSTM, combined with sparsity-inducing regularization, to infer Granger causality. Building on similar ideas, Khanna and Tan (2019) proposed the economy statistical recurrent units (eSRU), applying the sparsity constraints on the first-layer weights of statistical recurrent units (SRU) to infer causal relationships. Bussmann, Nys, and Latré (2021) proposed the Neural Additive Vector Autoregression (NAVAR), including NAVAR(MLP) and NAVAR(LSTM), for Granger causality inference. Nauta, Bucur, and Seifert (2019) proposed the Temporal Causal Discovery Framework (TCDF), which employs temporal convolutional networks (TCN) alongside a causal validation algorithm to both infer causal relationships and determine time lags. Addressing challenges in irregularly sampled time series, Cheng et al. (2023) proposed Causal Discovery from Irregular Time Series (CUTS), capable of uncovering Granger causality even when data contains random missing points or non-uniform sampling intervals. To further enhance this ability, Cheng et al. (2024a) proposed CUTS+, which incorporates a coarse-to-fine causal discovery strategy and a message-passing graph neural network to improve the performance of causal inference and address limitations such as large causal graphs and redundant data prediction in CUTS. Marcinkevics and Vogt (2021) proposed the generalized vector autoregression (GVAR) model, grounded in a self-explaining neural network architecture, offering both effective causal discovery and enhanced model interpretability. Suryadi, Chew, and Ong (2023) proposed Jacobian Granger

causality (JGC), which utilizes the Jacobian matrix to measure variable importance, and introduced a variable selection procedure based on significance and consistency criteria to identify Granger causality.

Preliminary

Time series Granger causality inference

We inherit the notation in (Cheng et al. 2024a) and denote a multivariate time series as $X = \{x_{T,i}\}_{i=1}^p$, where $x_{t,i}$ is the t^{th} time point of the series i , and $t \in \{1, \dots, T\}$, $i \in \{1, \dots, p\}$, with T is the total sampling points, p is the dimension of the time series. According to the nonlinear autoregressive model, $x_{t,i}$ can be denoted as a combination of the time series past values:

$$x_{t,i} = f_i(x_{t-k:t-1,1}, x_{t-k:t-1,2}, \dots, x_{t-k:t-1,p}) + e_{t,i} \quad (1)$$

where $x_{t-k:t-1,i}$ is the past value of series i , k is the maximum time lag, $e_{t,i}$ is an independent noise item, f_i usually takes the form of the neural network or other nonlinear function.

Since the prediction of $x_{t,i}$ depends on the historical information of other time series, if the past values of a series x_j can significantly enhance the prediction of the future values of x_i , then x_j is Granger-cause to x_i ($x_j \rightarrow x_i$); otherwise, x_j is consider no Granger-cause to x_i ($x_j \nrightarrow x_i$).

Kolmogorov-Arnold Network (KAN)

KAN is first proposed by Liu et al. (2024), which has emerged as an attractive alternative to MLP. Different from

MLP, whose theoretical foundation is established by the universal approximation theorem, KAN is based on the Kolmogorov-Arnold (KA) representation theorem. This theorem posits that any multivariate continuous function can be expressed as the sum of a finite set of univariate functions: Let $f : [0, 1]^n \rightarrow \mathbb{R}$ be a continuous multivariate function. There exist continuous univariate functions Φ_q and $\phi_{q,p}$ such that:

$$f(x_1, x_2, \dots, x_n) = \sum_{q=1}^{2n+1} \Phi_q \left(\sum_{p=1}^n \phi_{q,p}(x_p) \right) \quad (2)$$

where $\Phi_i : \mathbb{R} \rightarrow \mathbb{R}$ and $\phi_{q,p} : [0, 1] \rightarrow \mathbb{R}$ are continuous functions.

Before the work of Liu et al. (2024), the application of the KA representation theorem in deep learning was quite limited. This is mainly due to two challenges: (1) The function $\phi_{q,p}$ is often non-smooth. (2) The theorem mainly supports the construction of two-layer networks with a restricted number of hidden units. Therefore, instead of rigidly enforcing KA representation theorem, Liu et al. (2024) expand the network design to allow arbitrary depth and width, making it more suitable for deep learning tasks.

GRNGC

KAN-based time series prediction

As Granger causality is fundamentally grounded in prediction, time series forecasting models are commonly utilized to construct causal inference frameworks. Inspired by the recent success of KAN in time series modelling, we construct GCNGC using KAN in this section, which can be denoted as follows:

KAN contains $L - 1$ layers, and h^l is denoted as the l^{th} hidden layer. The trainable parameter of KAN including base weight W_b and spline weight W_s on each layer. By using these notations, the vector of the hidden units in the first layer h^1 is denoted as:

$$\mathbf{h}^1 = \underbrace{\begin{pmatrix} \phi_{0,1,1}(\cdot) & \cdots & \phi_{0,1,n_0}(\cdot) \\ \phi_{0,2,1}(\cdot) & \cdots & \phi_{0,2,n_0}(\cdot) \\ \vdots & \vdots & \vdots \\ \phi_{0,n_1,1}(\cdot) & \cdots & \phi_{0,n_1,n_0}(\cdot) \end{pmatrix}}_{\Phi_0} x_{t-k:t-1,1:p} \quad (3)$$

where n_0 is the input time series dimension, n_1 is the first hidden layer size. Here, the $\phi(x)$ is denoted as:

$$\phi(x) = W_b^0 \cdot \frac{x}{1 + e^{-x}} + W_s^0 \cdot \sum_i c_i B_i(x) \quad (4)$$

where B_i is denoted as B-splines, c_i is the control coefficients, W_b^0 and W_s^0 are the first layer weight of W_b and W_s , respectively. Subsequently, The vector of the hidden units in the layer l is denoted as:

$$\mathbf{h}^l = \underbrace{\begin{pmatrix} \phi_{l-1,1,1}(\cdot) & \cdots & \phi_{l-1,1,n_{l-1}}(\cdot) \\ \phi_{l-1,2,1}(\cdot) & \cdots & \phi_{l-1,2,n_{l-1}}(\cdot) \\ \vdots & \vdots & \vdots \\ \phi_{l-1,n_l,1}(\cdot) & \cdots & \phi_{l-1,n_l,n_{l-1}}(\cdot) \end{pmatrix}}_{\Phi_{l-1}} \mathbf{h}^{l-1} \quad (5)$$

where n_l and n_{l-1} is the l^{th} and $l-1^{th}$ hidden layer size, respectively. Here, the $\phi(x)$ is denoted as:

$$\phi(x) = W_b^{l-1} \cdot \frac{x}{1 + e^{-x}} + W_s^{l-1} \cdot \sum_i c_i B_i(x) \quad (6)$$

where W_b^{l-1} and W_s^{l-1} are the l^{th} layer weight of W_b and W_s , respectively. The input time series $x_{t-k:t-1,1:p}$ go through the $L-1$ hidden layers to generate the output $\hat{x}_{t,1:p}$, which is denoted as:

$$\hat{x}_{t,1:p} = \text{KAN}(x_{t-k:t-1,1:p}) = \Phi_{L-1} \circ h^{L-1} + e_t \quad (7)$$

Then, the predicted loss is defined as:

$$\mathcal{L}_p = \frac{1}{T-k} \sum_{t=k+1}^T (\hat{x}_{t,1:p} - x_{t-k:t-1,1:p})^2 \quad (8)$$

Granger causality inference

After constructing the time series forecasting model, it is essential to incorporate sparsity constraints to infer Granger causality. In this section, we propose a novel approach to extract causal relationships from neural networks instead of the traditional first-layer weights.

Specifically, for each time series j , the predicted values across all time steps are summed into a scalar function, which is denoted as:

$$s_j = \sum_{t=k+1}^T \hat{x}_{t,j} \quad (9)$$

Subsequently, for each scalar function s_j , the gradient is computed with respect to every element of the input time series $x_{t-k:t-1,1:p}$, which is denoted as:

$$g_j = \nabla_{x_{t-k:t-1,1:p}} s_j = \begin{bmatrix} \frac{\partial s_j}{\partial x_{t-k,1}} & \cdots & \frac{\partial s_j}{\partial x_{t-k,p}} \\ \vdots & \vdots & \vdots \\ \frac{\partial s_j}{\partial x_{t-1,1}} & \cdots & \frac{\partial s_j}{\partial x_{t-1,p}} \end{bmatrix} \in \mathbb{R}^{(T-k) \times p} \quad (10)$$

To obtain the sparse Granger causality matrix, we first compute the average of g_j over the temporal domain to construct the j^{th} row of the Granger causality matrix GC_{avg} :

$$GC_{avg}(j, :) = \frac{1}{T-k} \sum_{t=k+1}^T |g_j(t, :)| \in \mathbb{R}^p \quad (11)$$

Then, L_1 regularization is imposed on $GC_{avg}(j, :)$ to sparse its elements, which is denoted as:

$$\|GC_{avg}(j, :)\|_1 \quad (12)$$

where $\|\cdot\|_1$ is denoted as the L_1 norm. Therefore, the total sparsity-inducing loss \mathcal{L}_s is defined as:

$$\mathcal{L}_s = \lambda \sum_{j=1}^p \|GC_{avg}(j, :)\|_1 \quad (13)$$

where $\lambda > 0$ is the sparsity-inducing hyperparameter that controls the regularization strength. Finally, the loss function is defined as:

$$\mathcal{L} = \mathcal{L}_p + \mathcal{L}_s \quad (14)$$

Numerical Experiment

In this section, we compare GRNGC with nine state-of-the-art models, including cMLP & cLSTM (Tank et al. 2018), TCDF (Nauta, Bucur, and Seifert 2019), eSRU (Khanna and Tan 2019), GVAR (Marcinkevičs and Vogt 2021), PCMCi (Runge et al. 2019), JGC (Suryadi, Chew, and Ong 2023), CR-VAE (Li, Yu, and Principe 2023), and CUTS+ (Cheng et al. 2024a), across four widely used benchmark datasets: DREAM in Silico Network Challenge (Madar et al. 2010), Lorenz-96 (Karimi and Paul 2010), fMRI BOLD signal (Smith et al. 2011), and CausalTime (Cheng et al. 2024b).

Consistent with previous research, model performance is assessed through the Area Under the Receiver Operating Characteristic Curve (AUROC) and the Area Under the Precision-Recall Curve (AUPRC). In the context of gene regulatory network analysis, evaluation is confined to the off-diagonal elements of the Granger causality matrix, as the ground truth causal matrix does not account for self-causality. For other datasets, performance evaluation is conducted on the full adjacency matrix. The detailed hyperparameters and tuning strategies are provided in the Supplementary materials.

DREAM in Silico Network Challenge

The DREAM in Silico Network Challenge consists of DREAM3 and DREAM4 datasets. DREAM3 comprises five sub-datasets, two for *Escherichia coli* (*E.coli-1*, *E.coli-2*) and three for Yeast (*Yeast-1*, *Yeast-2*, *Yeast-3*). Each sub-dataset contains 100 time series, with 21 sampling points per series, and is replicated 46 times, resulting in a total of 966 sampling points. Similarly, the DREAM4 dataset also contains five sub-datasets. However, each time series includes only 210 sampling points.

Table 1: AUROC of DREAM3 dataset, $T = 966$, $p = 100$

Models	AUROC				
	Ecoli-1	Ecoli-2	Yeast-1	Yeast-2	Yeast-3
cMLP	0.648	0.568	0.585	0.511	0.531
cLSTM	0.651	0.609	0.579	0.524	0.552
TCDF	0.615	0.621	0.581	0.567	0.565
eSRU	0.660	0.636	0.631	0.561	0.559
GVAR	0.652	0.634	0.623	0.570	0.554
PCMCi	0.557	0.577	0.652	0.573	0.548
JGC	0.522	0.536	0.611	0.558	0.531
CR-VAE	0.557	0.577	0.652	0.573	0.548
CUTS+	0.703	0.669	0.643	0.581	0.554
GRNGC	0.728	0.671	0.661	0.567	0.575
True variable usage	1.25%	1.19%	1.66%	3.89%	5.51%

The AUROCs of DREAM3 and DREAM4 datasets are shown in Tables 1 and 2. The corresponding AUPRC results are provided supplementary material. For the DREAM3 dataset, GRNGC achieves the highest AUROC in four out of five sub-datasets (*E.coli-1*, *E.coli-2*, *Yeast-1*, *Yeast-3*). In the DREAM4 dataset, GRNGC achieves the highest AUROC in all five sub-datasets. Additionally, the AUPRC results indicate that the proposed model exhibits superior performance in inferring sparse causal relationships. These findings col-

Table 2: AUROC of DREAM4 dataset, $T = 210$, $p = 100$

Models	AUROC				
	Gene-1	Gene-2	Gene-3	Gene-4	Gene-5
cMLP	0.652	0.522	0.509	0.511	0.531
cLSTM	0.633	0.509	0.498	0.524	0.552
TCDF	0.598	0.491	0.467	0.567	0.565
eSRU	0.647	0.554	0.545	0.561	0.559
GVAR	0.662	0.569	0.565	0.578	0.554
PCMCi	0.591	0.522	0.507	0.543	0.548
JGC	0.544	0.502	0.513	0.505	0.517
CR-VAE	0.583	0.534	0.536	0.529	0.545
CUTS+	0.738	0.622	0.591	0.584	0.594
GRNGC	0.782	0.718	0.670	0.683	0.701
True variable usage	1.77%	2.51%	1.96%	2.13%	1.94%

lectively highlight the effectiveness of GRNGC in inferring Granger causality from high-dimensional time series.

Lorenz-96

Lorenz-96 is formulated as the following ordinary differential equation:

$$\frac{\partial x_{t,i}}{\partial t} = -x_{t,i-1} (x_{t,i-2} - x_{t,i+1}) - x_{t,i} + F \quad (15)$$

where F represents the forcing term applied to the system, $i = 1, 2, \dots, p$, p is the dimension of time series. For each time series i , the corresponding $x_{t,i}$ is influenced by four variables: $i-1$, $i-2$, i , and $i+1$. In our study, to investigate the model’s performance on high-dimensional time series, we set $p = 100$, $F = \{10, 20, 40\}$, and $T = 1000$.

Table 3 presents the performance of each model under three different forcing terms in the Lorenz-96 system. When $F = 10$, all models except TCDF and CR-VAE effectively infer causal relationships, with GRNGC, eSRU, and CUTS+ achieving the best scores (AUROC and AUPRC = 1.0). As F increases to 20 and 40, the time series exhibit more pronounced chaotic dynamics and heightened non-linearity, making causal inference more challenging. Under these more complex conditions, GRNGC consistently attains the highest AUROC and AUPRC, demonstrating its robustness and effectiveness on the Lorenz-96 dataset.

fMRI BOLD

To further evaluate the model’s performance under the condition of limited sample points, we conducted experiments using the first 5 subjects from the Sim3 subset of the fMRI BOLD. Sim3 comprises 15 time series, each containing only 200 time points, with a true variable usage of 14.67%.

As shown in Table 4, although JGC achieves the highest AUROC, its AUPRC is significantly lower than that of the other models. In contrast, GRNGC demonstrates a competitive AUROC while also achieving the best performance in AUPRC, suggesting a more balanced and robust performance in both evaluation metrics.

CausalTime

CausalTime is a benchmark dataset recently introduced by Cheng et al. (2024b), comprising three sub-datasets: AQI

Table 3: AUROC and AUPRC of the Lorenz-96 dataset, $p = 100$, $T = 1000$. We highlight the best and the second best in bold and with underlining, respectively.

Models	$F = 10$		$F = 20$		$F = 40$	
	AUROC (\uparrow)	AUPRC (\uparrow)	AUROC (\uparrow)	AUPRC (\uparrow)	AUROC (\uparrow)	AUPRC (\uparrow)
cMLP	<u>0.995\pm0.003</u>	<u>0.992\pm0.003</u>	0.993 \pm 0.004	0.978 \pm 0.004	0.972 \pm 0.005	0.943 \pm 0.006
cLSTM	<u>0.983\pm0.008</u>	<u>0.961\pm0.012</u>	0.932 \pm 0.008	0.904 \pm 0.009	0.876 \pm 0.007	0.839 \pm 0.011
TCDF	0.852 \pm 0.036	0.733 \pm 0.041	0.728 \pm 0.027	0.587 \pm 0.033	0.585 \pm 0.046	0.439 \pm 0.052
eSRU	1.000\pm0.000	1.000\pm0.000	<u>0.996\pm0.001</u>	<u>0.991\pm0.002</u>	0.988 \pm 0.003	0.954 \pm 0.005
GVAR	0.996 \pm 0.002	0.994 \pm 0.003	<u>0.992\pm0.002</u>	<u>0.983\pm0.004</u>	0.975 \pm 0.005	0.946 \pm 0.008
PCMCi	0.956 \pm 0.006	0.932 \pm 0.005	0.921 \pm 0.006	0.887 \pm 0.007	0.896 \pm 0.005	0.853 \pm 0.008
JGC	0.985 \pm 0.005	0.981 \pm 0.004	0.956 \pm 0.007	0.962 \pm 0.004	0.947 \pm 0.008	0.936 \pm 0.012
CR-VAE	0.876 \pm 0.022	0.761 \pm 0.035	0.755 \pm 0.036	0.640 \pm 0.037	0.639 \pm 0.032	0.528 \pm 0.047
CUTS+	1.000\pm0.000	1.000\pm0.000	1.000\pm0.000	1.000\pm0.000	<u>0.991\pm0.002</u>	<u>0.967\pm0.003</u>
GRNGC	1.000\pm0.000	1.000\pm0.000	1.000\pm0.000	1.000\pm0.000	0.997\pm0.001	0.975\pm0.004
True variable usage			40%			

Table 4: AUROC and AUPRC of the fMRI BOLD dataset, $p = 15$, $T = 200$. We highlight the best and the second best in bold and with underlining, respectively.

Models	AUROC (\uparrow)	AUPRC (\uparrow)
cMLP	0.805 \pm 0.015	0.658 \pm 0.035
cLSTM	0.714 \pm 0.027	0.633 \pm 0.047
TCDF	0.763 \pm 0.037	0.661 \pm 0.059
eSRU	0.825 \pm 0.027	0.685 \pm 0.046
GVAR	0.804 \pm 0.018	0.672 \pm 0.085
PCMCi	0.735 \pm 0.031	0.529 \pm 0.074
JGC	0.867\pm0.008	0.547 \pm 0.063
CR-VAE	0.579 \pm 0.011	0.397 \pm 0.077
CUTS+	0.836 \pm 0.014	<u>0.705\pm0.063</u>
GRNGC	<u>0.841\pm0.032</u>	0.712\pm0.047
True variable usage		14.67%

($p = 72$), Traffic ($p = 40$), and Medical ($p = 40$). The time series of each dataset contains 19200 time points. The evaluation metrics, AUROC and AUPRC, are computed following the experimental setting of Cheng et al. (2024b). Moreover, the performances of other models (including Granger causality (GC, (Granger 1969)), Vector autoregressive (VAR, (Stock and Watson 2001)), NTS-NOTEARS (N.NTS, (Sun et al. 2023)), Rhino (Gong et al. 2022), Neural Graphical Model (NGM, (Bellot, Branson, and van der Schaar 2021)), Latent Convergent Cross Mapping (LCCM, (De Brouwer et al. 2020)), Scalable Causal Graph Learning (SCGL, (Xu, Huang, and Yoo 2019)), and CUTS) are directly adopted from the CausalTime study, which systematically benchmarks recent representative state-of-the-art causal inference methods on this dataset.

As shown in Table 5, the proposed GRNGC achieves the best performances on the Traffic and Medical datasets, outperforming other baseline models. Notably, GRNGC is the only model with AUROC and AUPRC >0.9 on the medi-

cal dataset. In the AQI dataset, GRNGC is slightly below CUTS+ in terms of AUROC and behind LCCM, CUTS+, and SVAR in AUPRC. Nevertheless, it exhibits consistent reliability and robustness across all datasets, achieving metrics significantly above the threshold of 0.5.

Ablation studies

The ablation studies are conducted to evaluate the individual contributions of each component within our model to overall performance, deriving insights into the impact of the model’s fundamental elements on Granger causality inference. Three sub-datasets are selected: Lorenz-96 ($F = 10$, $p = 100$), DREAM4, and Medical. We evaluate how changing the number of hidden units affects the model performance. Moreover, GRNGC can be constructed using various time series prediction models and does not depend on a specific model. Therefore, we replace KAN with MLP, LSTM, and Temporal Convolutional Network (TCN) to evaluate its performance under different time series prediction models. The corresponding results are presented in Table 6 and 7.

The results indicate that varying the number of hidden layer units has minimal impact on the performance of the DREAM4 and Medical datasets. However, in the Lorenz-96 dataset, an insufficient number of hidden units leads to a marked decline in AUPRC. Regarding the time series prediction models, MLP performs comparably to KAN and even outperforms it in terms of AUROC on the DREAM4 dataset. While TCN and LSTM perform well on the Lorenz-96 and Medical datasets, they lag behind MLP and KAN on the DREAM4 dataset. These results highlight the robustness and scalability of GRNGC across diverse settings and underscore the necessity of tailoring the model to the specific characteristics of each dataset.

Model complexity

The proposed GRNGC uses only a single model rather than the component-wise architecture, which significantly

Table 5: AUROC and AUPRC of the CausalTime dataset, $p = 72/40/40$, $T = 19200$. We highlight the best and the second best in bold and with underlining, respectively.

Models	AQI		Traffic		Medical	
	AUROC	AUPRC	AUROC	AUPRC	AUROC	AUPRC
GC	0.4538 \pm 0.0377	0.6347 \pm 0.0158	0.4191 \pm 0.0310	0.2789 \pm 0.0018	0.5737 \pm 0.0338	0.4213 \pm 0.0281
VAR	0.6225 \pm 0.0406	0.7903 \pm 0.0175	0.6329 \pm 0.0047	0.5845 \pm 0.0021	0.7130 \pm 0.0188	0.6774 \pm 0.0358
N.NTS	0.5729 \pm 0.0229	0.7100 \pm 0.0228	<u>0.6452\pm0.0335</u>	0.5770 \pm 0.0542	0.5019 \pm 0.0682	0.4567 \pm 0.0162
PCMCi	0.5272 \pm 0.0744	0.6734 \pm 0.0372	<u>0.5422\pm0.0737</u>	0.3474 \pm 0.0581	0.6991 \pm 0.0111	0.5082 \pm 0.0177
Rhino	0.6700 \pm 0.0983	0.7593 \pm 0.0755	0.6274 \pm 0.0185	0.3772 \pm 0.0093	0.6520 \pm 0.0212	0.4897 \pm 0.0321
NGM	0.6728 \pm 0.0164	0.4786 \pm 0.0196	0.4660 \pm 0.0144	0.2826 \pm 0.0098	0.5551 \pm 0.0154	0.4697 \pm 0.0166
LCCM	0.8565 \pm 0.0653	0.9260\pm0.0246	0.5545 \pm 0.0254	0.5907 \pm 0.0475	0.8013 \pm 0.0218	<u>0.7554\pm0.0235</u>
SCGL	0.4915 \pm 0.0476	0.3584 \pm 0.0281	0.5927 \pm 0.0553	0.4544 \pm 0.0281	0.5019 \pm 0.0224	0.4833 \pm 0.0185
cMLP	0.6453 \pm 0.0135	0.6566 \pm 0.0134	0.5514 \pm 0.0283	0.2561 \pm 0.0311	0.5744 \pm 0.0096	0.4637 \pm 0.0121
cLSTM	0.7172 \pm 0.0076	0.7177 \pm 0.0069	0.6032 \pm 0.0056	0.3583 \pm 0.0495	0.5315 \pm 0.0151	0.4268 \pm 0.0255
TCDF	0.4148 \pm 0.0207	0.6527 \pm 0.0087	0.5029 \pm 0.0041	0.3637 \pm 0.0087	0.6329 \pm 0.0384	0.5544 \pm 0.0313
eSRU	0.8229 \pm 0.0317	0.7223 \pm 0.0317	0.5987 \pm 0.0192	0.4886 \pm 0.0317	0.7559 \pm 0.0365	0.7352 \pm 0.0600
GVAR	0.6437 \pm 0.0259	0.6573 \pm 0.0474	0.5361 \pm 0.0283	0.3795 \pm 0.0471	0.6882 \pm 0.0263	0.6498 \pm 0.0452
JGC	0.5017 \pm 0.0352	0.5547 \pm 0.0343	0.5372 \pm 0.0475	0.3549 \pm 0.0252	0.5383 \pm 0.0118	0.5271 \pm 0.0134
CR-VAE	0.6754 \pm 0.0118	0.7201 \pm 0.0267	0.6049 \pm 0.0363	0.3760 \pm 0.0348	0.5563 \pm 0.0214	0.5891 \pm 0.0157
CUTS	0.6013 \pm 0.0038	0.5096 \pm 0.0362	0.6238 \pm 0.0179	0.1525 \pm 0.0226	0.3739 \pm 0.0297	0.1537 \pm 0.0039
CUTS+	0.8928\pm0.0213	<u>0.7983\pm0.0875</u>	0.6175 \pm 0.0752	<u>0.6367\pm0.1197</u>	<u>0.8202\pm0.0173</u>	0.5481 \pm 0.1349
GRNGC	<u>0.8729\pm0.0137</u>	0.7329 \pm 0.0341	0.7730\pm0.0152	0.6395\pm0.0145	0.9194\pm0.0141	0.9047\pm0.0196
True variable usage	28.08%		20.5%		38.25%	

Table 6: Ablation study comparing the performance of GRNGC with different number of hidden units H .

Models	Lorenz-96		DREAM4		Medical	
	AUROC	AUPRC	AUROC	AUPRC	AUROC	AUPRC
$H = 32$	0.969 \pm 0.003	0.667 \pm 0.023	0.693 \pm 0.049	0.085 \pm 0.067	0.891 \pm 0.012	0.853 \pm 0.024
$H = 64$	0.994 \pm 0.002	0.858 \pm 0.003	0.698 \pm 0.048	0.092 \pm 0.028	0.912 \pm 0.017	0.891 \pm 0.023
$H = 128$	1.000 \pm 0.000	1.000 \pm 0.000	0.711 \pm 0.043	0.115 \pm 0.036	0.914 \pm 0.018	0.890 \pm 0.021
$H = 256$	1.000 \pm 0.000	1.000 \pm 0.000	0.710 \pm 0.039	0.116 \pm 0.044	0.919 \pm 0.014	0.904 \pm 0.019
$H = 512$	1.000 \pm 0.000	1.000 \pm 0.000	0.702 \pm 0.045	0.111 \pm 0.043	0.883 \pm 0.028	0.876 \pm 0.037

reduces computational overhead. Fig.2 presents the comparison of GRNGC (KAN) and GRNGC (MLP) with other models in terms of AUROC, AUPRC, and the number of tunable parameters on the DREAM4 (Gene 1) dataset.

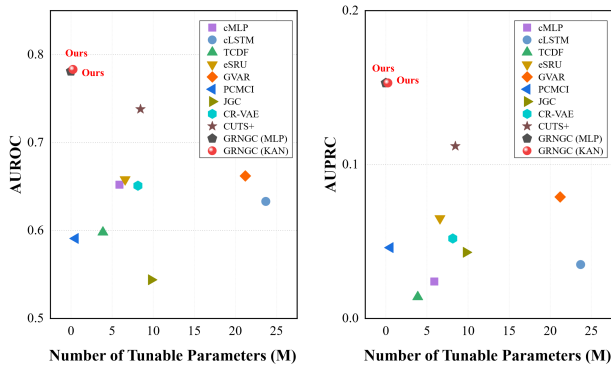


Figure 2: Performance comparisons on DREAM4 (Gene-1): AUROC, AUPRC, and the number of tunable parameters.

Owing to its simplified architecture, GRNGC contains fewer tunable parameters compared to all existing models. Moreover, replacing KAN with MLP further reduces the total number of parameters, with minimal impact on AUROC and AUPRC. As a result, GRNGC achieves improved inference efficiency while significantly lowering computational overhead.

Reconstruction of real-world gene regulatory networks

Real-world networks often exhibit complex nonlinear dynamics, making their causal structures inherently difficult to infer. Therefore, in this section, we focus on gene regulatory networks within biological systems and evaluate the performance of GRNGC on four real-world gene regulatory network datasets:

- *SOS DNA repair network (SOS)*: The SOS dataset is a real dataset validated in E.coli (Shen-Orr et al. 2002), comprising 9 genes and 24 regulatory interactions.
- *Yeast cell (Yeast)*: This dataset was retrieved from the Gene Expression Omnibus (GEO) under accession num-

Table 7: Ablation study on changing time series prediction model in GRNGC.

Models	Lorenz-96		DREAM4		Medical	
	AUROC	AUPRC	AUROC	AUPRC	AUROC	AUPRC
KAN	1.000 \pm 0.000	1.000 \pm 0.000	0.711 \pm 0.043	0.115 \pm 0.036	0.919 \pm 0.014	0.904 \pm 0.019
MLP	1.000 \pm 0.000	0.997 \pm 0.001	0.712 \pm 0.058	0.109 \pm 0.051	0.917 \pm 0.015	0.902 \pm 0.018
LSTM	0.994 \pm 0.002	0.985 \pm 0.004	0.652 \pm 0.047	0.087 \pm 0.043	0.853 \pm 0.017	0.829 \pm 0.022
TCN	0.998 \pm 0.001	0.995 \pm 0.002	0.639 \pm 0.079	0.064 \pm 0.062	0.882 \pm 0.024	0.866 \pm 0.027

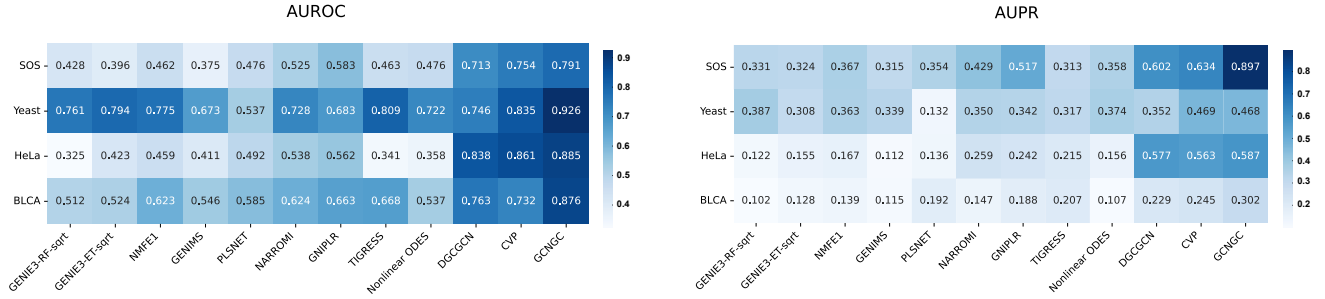


Figure 3: AUROC and AUPRC comparisons on *SOS*, *Yeast*, *HeLa*, and *BLCA* gene express datasets.

ber GSE8799 (Yalamanchili et al. 2014). It comprises gene expression time series data for yeast, involving 8 genes and 6 regulatory interactions.

- *Human HeLa cell (HeLa)*: The HeLa dataset is derived from gene expression profiles of the HeLa cell cycle (Whitfield et al. 2002). Based on this data, Sambo et al. (2008) reported a subnetwork of 9 genes and 9 regulatory interactions and the corresponding time series.
- *Bladder Urothelial Carcinoma (BLCA)*: The BLCA dataset is derived from the hsa05219 pathway of the Kyoto Encyclopedia of Genes and Genomes (KEGG). By integrating gene data from this pathway with transcriptomic profiles of BLCA from The Cancer Genome Atlas (TCGA), a regulatory network consisting of 10 genes and 7 interactions was constructed (Zhang et al. 2015).

Since GRNGC outperforms other causal inference models on pervious simulated gene regulatory network datasets (DREAM3 & DREAM4), we exclude these models for comparison in this section. Instead, we focus on benchmarking GRNGC against methods developed for gene regulatory network, including GENIE-RF-sqrt and GENIE-ET-sqrt (Huynh-Thu et al. 2010), NIMEFI (Ruyssinck et al. 2014), GENIMS (Wu et al. 2016), PLSNET (Guo et al. 2016), NARROMI (Zhang et al. 2013), GNIPLR (Zhang, Chang, and Liu 2021), TIGRESS (Haury et al. 2012), Nonlinear ODES (Ma, Fang, and Jiao 2020), DGCGRN (Wei et al. 2024), and CVP (Zhang et al. 2025).

As shown in Fig.3, GRNGC consistently exhibits superior performance across four real-world gene expression datasets. On the *SOS* dataset, it achieves AUROC scores

comparable to those of CVP and DGCGCN, and outperforms CVP in AUPR by 27%. For the *Yeast* and *BLCA* datasets, GRNGC exceeds the second-best model by approximately 10% in AUROC. In the *HeLa* dataset, GRNGC performs on par with CVP and DGCGCN in both AUROC and AUPR. These results highlight the model’s robust ability to uncover causal relationships from real biological data.

Conclusion

In this study, we propose Gradient Regularization-based Neural Granger Causality (GRNGC), a novel framework for inferring causal relationships from time series. Different from previous models that rely on the component-wise architecture and derive causality from the first-layer weights of the neural network, GRNGC employs a single model and extracts causal dependencies directly from the gradients between inputs and outputs. This design enhances the model’s capacity to capture complex causal relationships and significantly reduces computational cost. Moreover, GRNGC is model-agnostic and can be constructed with various time series forecasting architectures, such as KAN, MLP, and LSTM, thereby offering greater flexibility in its application. Extensive experiments on DREAM, Lorenz-96, fMRI BOLD, and CausalTime demonstrate the superior performance of GRNGC over existing baselines. In real-world genetic datasets, GRNGC outperforms specialized gene regulatory network models and can be used to discover underlying regulatory interactions. The Pytorch code of GRNGC is anonymized and uploaded to the Supplementary Materials.

References

- Bellot, A.; Branson, K.; and van der Schaar, M. 2021. Neural graphical modelling in continuous-time: consistency guarantees and algorithms. In *International Conference on Learning Representations*.
- Bussmann, B.; Nys, J.; and Latré, S. 2021. Neural additive vector autoregression models for causal discovery in time series. In *Discovery Science: 24th International Conference, DS 2021, Halifax, NS, Canada, October 11–13, 2021, Proceedings 24*, 446–460. Springer.
- Cheng, Y.; Li, L.; Xiao, T.; Li, Z.; Suo, J.; He, K.; and Dai, Q. 2024a. CUTS+: High-dimensional causal discovery from irregular time-series. In *Proceedings of the AAAI Conference on Artificial Intelligence*, volume 38, 11525–11533.
- Cheng, Y.; Wang, Z.; Xiao, T.; Zhong, Q.; Suo, J.; and He, K. 2024b. CausalTime: Realistically Generated Time-series for Benchmarking of Causal Discovery. In *The Twelfth International Conference on Learning Representations*.
- Cheng, Y.; Yang, R.; Xiao, T.; Li, Z.; Suo, J.; He, K.; and Dai, Q. 2023. CUTS: Neural Causal Discovery from Irregular Time-Series Data. In *The Eleventh International Conference on Learning Representations*.
- De Brouwer, E.; Arany, A.; Simm, J.; and Moreau, Y. 2020. Latent convergent cross mapping. In *International Conference on Learning Representations*.
- Gong, W.; Jennings, J.; Zhang, C.; and Pawlowski, N. 2022. Rhino: Deep Causal Temporal Relationship Learning with History-dependent Noise. In *The Eleventh International Conference on Learning Representations*.
- Granger, C. W. 1969. Investigating causal relations by econometric models and cross-spectral methods. *Econometrica: journal of the Econometric Society*, 424–438.
- Guo, S.; Jiang, Q.; Chen, L.; and Guo, D. 2016. Gene regulatory network inference using PLS-based methods. *BMC bioinformatics*, 17: 1–10.
- Hauray, A.-C.; Mordelet, F.; Vera-Licona, P.; and Vert, J.-P. 2012. TIGRESS: trustful inference of gene regulation using stability selection. *BMC systems biology*, 6: 1–17.
- Huynh-Thu, V. A.; Irrthum, A.; Wehenkel, L.; and Geurts, P. 2010. Inferring regulatory networks from expression data using tree-based methods. *PloS one*, 5(9): e12776.
- Karimi, A.; and Paul, M. R. 2010. Extensive chaos in the Lorenz-96 model. *Chaos: An interdisciplinary journal of nonlinear science*, 20(4).
- Khanna, S.; and Tan, V. Y. 2019. Economy Statistical Recurrent Units For Inferring Nonlinear Granger Causality. In *International Conference on Learning Representations*.
- Li, H.; Yu, S.; and Principe, J. 2023. Causal recurrent variational autoencoder for medical time series generation. In *Proceedings of the AAAI conference on artificial intelligence*, volume 37, 8562–8570.
- Liu, Z.; Wang, Y.; Vaidya, S.; Ruehle, F.; Halverson, J.; Soljačić, M.; Hou, T. Y.; and Tegmark, M. 2024. Kan: Kolmogorov-arnold networks. *arXiv preprint arXiv:2404.19756*.
- Ma, B.; Fang, M.; and Jiao, X. 2020. Inference of gene regulatory networks based on nonlinear ordinary differential equations. *Bioinformatics*, 36(19): 4885–4893.
- Madar, A.; Greenfield, A.; Vanden-Eijnden, E.; and Bonneau, R. 2010. DREAM3: network inference using dynamic context likelihood of relatedness and the inferelator. *PloS one*, 5(3): e9803.
- Marcinkevičs, R.; and Vogt, J. E. 2021. Interpretable Models for Granger Causality Using Self-explaining Neural Networks. In *International Conference on Learning Representations (ICLR 2021)*. OpenReview.
- Nauta, M.; Bucur, D.; and Seifert, C. 2019. Causal discovery with attention-based convolutional neural networks. *Machine Learning and Knowledge Extraction*, 1(1): 19.
- Runge, J.; Nowack, P.; Kretschmer, M.; Flaxman, S.; and Sejdinovic, D. 2019. Detecting and quantifying causal associations in large nonlinear time series datasets. *Science advances*, 5(11): eaau4996.
- Ruyssinck, J.; Huynh-Thu, V. A.; Geurts, P.; Dhaene, T.; De-meester, P.; and Saeys, Y. 2014. NIMEFI: gene regulatory network inference using multiple ensemble feature importance algorithms. *PLoS One*, 9(3): e92709.
- Sambo, F.; Di Camillo, B.; Toffolo, G.; et al. 2008. CNET: an algorithm for reverse engineering of causal gene networks. *NETTAB2008, Varenna, Italy*.
- Shen-Orr, S. S.; Milo, R.; Mangan, S.; and Alon, U. 2002. Network motifs in the transcriptional regulation network of *Escherichia coli*. *Nature genetics*, 31(1): 64–68.
- Smith, S. M.; Miller, K. L.; Salimi-Khorshidi, G.; Webster, M.; Beckmann, C. F.; Nichols, T. E.; Ramsey, J. D.; and Woolrich, M. W. 2011. Network modelling methods for FMRI. *Neuroimage*, 54(2): 875–891.
- Stock, J. H.; and Watson, M. W. 2001. Vector autoregressions. *Journal of Economic perspectives*, 15(4): 101–115.
- Sun, X.; Schulte, O.; Liu, G.; and Poupart, P. 2023. NTS-NOTEARS: Learning Nonparametric DBNs With Prior Knowledge. In *International Conference on Artificial Intelligence and Statistics, 1942–1964*. PMLR.
- Suryadi, S.; Chew, L. Y.; and Ong, Y.-S. 2023. Granger causality using Jacobian in neural networks. *Chaos: An Interdisciplinary Journal of Nonlinear Science*, 33(2).
- Tank, A.; Covert, I.; Foti, N. J.; Shojaie, A.; and Fox, E. B. 2018. Neural Granger Causality for Nonlinear Time Series. *stat*, 1050: 16.
- Wei, P.-J.; Guo, Z.; Gao, Z.; Ding, Z.; Cao, R.-F.; Su, Y.; and Zheng, C.-H. 2024. Inference of gene regulatory networks based on directed graph convolutional networks. *Briefings in Bioinformatics*, 25(4): bbac309.
- Whitfield, M. L.; Sherlock, G.; Saldanha, A. J.; Murray, J. I.; Ball, C. A.; Alexander, K. E.; Matese, J. C.; Perou, C. M.; Hurt, M. M.; Brown, P. O.; et al. 2002. Identification of genes periodically expressed in the human cell cycle and their expression in tumors. *Molecular biology of the cell*, 13(6): 1977–2000.

- Wu, J.; Zhao, X.; Lin, Z.; and Shao, Z. 2016. Large scale gene regulatory network inference with a multi-level strategy. *Molecular Biosystems*, 12(2): 588–597.
- Xu, C.; Huang, H.; and Yoo, S. 2019. Scalable causal graph learning through a deep neural network. In *Proceedings of the 28th ACM international conference on information and knowledge management*, 1853–1862.
- Yalamanchili, H. K.; Yan, B.; Li, M. J.; Qin, J.; Zhao, Z.; Chin, F. Y.; and Wang, J. 2014. DDGni: dynamic delay gene-network inference from high-temporal data using gapped local alignment. *Bioinformatics*, 30(3): 377–383.
- Zhang, X.; Liu, K.; Liu, Z.-P.; Duval, B.; Richer, J.-M.; Zhao, X.-M.; Hao, J.-K.; and Chen, L. 2013. NARROMI: a noise and redundancy reduction technique improves accuracy of gene regulatory network inference. *Bioinformatics*, 29(1): 106–113.
- Zhang, X.; Zhao, J.; Hao, J.-K.; Zhao, X.-M.; and Chen, L. 2015. Conditional mutual inclusive information enables accurate quantification of associations in gene regulatory networks. *Nucleic acids research*, 43(5): e31–e31.
- Zhang, Y.; Chang, X.; and Liu, X. 2021. Inference of gene regulatory networks using pseudo-time series data. *Bioinformatics*, 37(16): 2423–2431.
- Zhang, Y.; Li, Q.; Wang, J.; Chang, X.; Chen, L.; and Liu, X. 2025. Causal network inference based on cross-validation predictability. *Communications Physics*, 8(1): 173.